

DNA-induced assembly of gold nanoprisms and polystyrene beads into 3D plasmonic SERS substrates

Emtias Chowdhury¹, Mohammad Shahinur Rahaman³ , Noppadon Sathitsuksanoh³ , Craig A Grapperhaus¹ and Martin G O'Toole² 

¹ Department of Chemistry, University of Louisville, Louisville, Kentucky, 40292, United States of America

² Department of Bioengineering, University of Louisville, Louisville, Kentucky, 40292, United States of America

³ Department of Chemical Engineering, University of Louisville, Louisville, Kentucky, 40292, United States of America

E-mail: martin.otoole@louisville.edu

Received 7 July 2020, revised 26 August 2020

Accepted for publication 27 September 2020

Published 14 October 2020



Abstract

The utilization of nanoparticle-polymer bead hybrid nanostructures as a SERS substrate depends on the control of the deposition, density, and distribution of nanoparticles on the bead surface. Here we demonstrate the fabrication of a large area SERS substrate via a two-step DNA mediated assembly of gold nanoprisms and polystyrene (PS) beads into a large ensemble of beads that are densely coated with nanoprisms. First, nanoprisms are loaded on PS beads through DNA hybridization. The close packed arrangement of anisotropic nanoprisms in different orientations on a bead surface results in a plasmonic substrate with a variable nanogap size ranging 1–20 nm. Nanoprisms-coated beads are then assembled into a large stack or aggregate of beads using a DNA-induced crystallization approach. Each aggregate consists of 20–50 nanoprisms-coated beads, leading to the formation of a large area of three-dimensional SERS substrate with a high-density of hot spots for SERS enhancement. An excellent enhancement factor (EF) of 1.09×10^5 and a very high detection sensitivity (up to 10^{-10} M) are observed for the analysis of a probe molecule (Methylene blue) using the SERS substrate.

Supplementary material for this article is available [online](#)

Keywords: surface enhanced raman spectroscopy, gold nanoprism, polystyrene bead, fluorescence quenching, SERS

(Some figures may appear in colour only in the online journal)

1. Introduction

Metal nanoparticle-based nanostructures have attracted significant attention due to their ability to concentrate localized surface plasmon resonance in a small volume, leading to remarkable enhancement of local electromagnetic fields [1]. This property enables the amplification of spectroscopic signals such as those associated with weak light–matter interactions and has been utilized for a broad array of

applications in plasmonics, including optical antennae [2], ultrasensitive sensors [3–5], plasmachemistry [6], chemical sensing [7], and information processing and communication [8], and most notably surface enhanced Raman scattering [9, 10]. In particular, anisotropic nanomaterials that exhibit unique shape-dependent properties and functionalities have been a subject of intense research for tuning plasmonic properties in these applications [11, 12]. As compared to spherical nanoparticles with surface plasmon resonances (SPR) of

relatively small wavelength range, the SPR of anisotropic particles i.e. gold/silver nanoprisms or nanorods are tunable throughout the visible and near-IR (NIR) regions of the spectrum based on their shape, aspect ratio and/or tip geometry of the nanoparticles [13–15]. Moreover, anisotropic gold/silver nanoprisms contain sharp edges and pointed or rounded vertices that confine electromagnetic field enhancement, which is highly relevant to many sensing applications, such as surface enhanced Raman scattering (SERS) based sensing [16]. When such nanoparticles are assembled in a predesigned spatial arrangement with gap sizes on the order of few nanometers, plasmonic hot spots are formed where the strongest enhancement of the Raman signal is expected to occur [17].

SERS activity and sensitivity relies upon huge electromagnetic field enhancements resulting from strong electromagnetic (EM) coupling of the SPRs between adjacent nanoparticles in close-packed metal nanostructures [18]. This strong electromagnetic coupling between nanoparticles leads to the formation of so-called nanogaps, where additional near field enhancement occurs, forming hot spots for SERS analysis [19]. These hot spots can provide extraordinary SERS enhancement, often sufficient for single molecule detection [20]. Several key factors that govern the strength of EM coupling and the overall SERS enhancement factor (EF) within the nanogap are gap distance, particle shape/size, and excitation configurations [21].

The dependence of SERS intensity on nanogap effects has led to the development of different experimental approaches to generate well defined assemblies of nanostructures with high density and reproducible hot spots, since uncontrolled and random aggregation leads to only isolated hot spots and discrepancies in SERS intensity [22]. Top down approaches such as electron-beam lithography (EBL) and focused ion-beam lithography (FIBL) have been developed to fabricate various type of plasmonic substrates with defined shape and tunable gap size for SERS applications [23–25]. However, these lithography-based techniques are expensive and time consuming. Moreover, it is challenging to apply these patterning techniques at nanoscale dimensions and at the surface of dispersed nanoparticle substrates [26]. In order to circumvent these shortcomings, bottom up fabrication methods such as molecular self-assembly have been used to construct various 2D and 3D nanostructures as SERS substrates [27–29]. Among self-assembly approaches, the utilization of DNA strands as a bottom-up self-assembly approach has emerged as a powerful tool to construct highly programable and complex plasmonic nanostructures in a predictable manner [30]. The molecular recognition, tunability, and predictability of DNA mediated interactions enables a high degree of control over particle assembly, thus allowing the fabrication of hot spot rich plasmonic SERS substrates with tunable nanogap sizes [17, 31]. For example, using DNA hybridization, gold nanospheres were assembled into various well defined and complex plasmonic nanostructures such as dimers or trimers [32], tetramers [33] and core satellite structures [34] that showed significant enhancement in SERS intensity. Furthermore, the use of DNA origami techniques has made possible the assembly of nanoprism bowtie configurations with a gap size of only

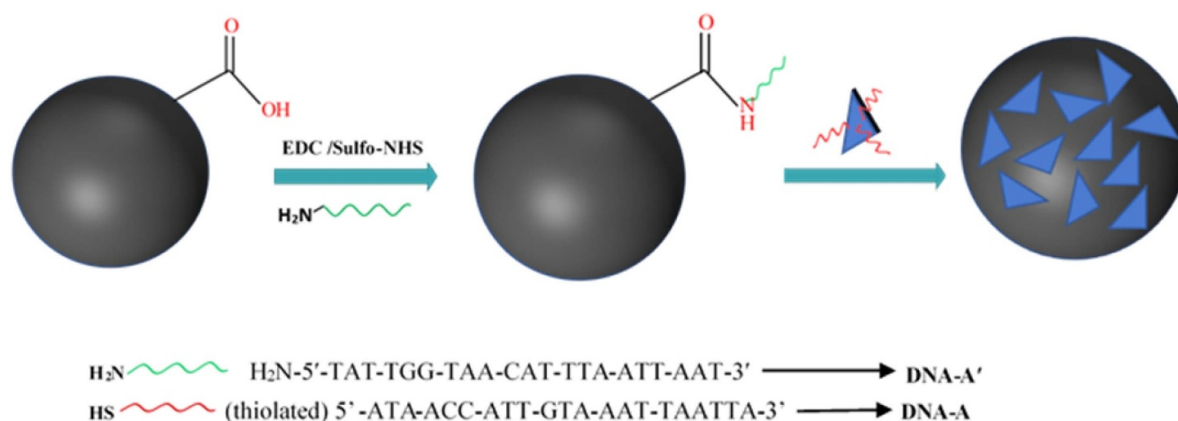
5 nm [35]. The tip-to-tip field coupling between nanoprisms produces strong electromagnetic field enhancement, which led to a mean SERS enhancement factor of about 2.6×10^9 and an electromagnetic field enhancement of about 2.3×10^3 .

The presence of a large number of hot spots at the focal volume of the Raman excitation laser are useful and desirable for SERS sensing [36]. In this context, the application of micron sized spherical polymer beads as a carrier medium or support for immobilizing metal nanoparticles has proven to be a useful tool for the fabrications of large areas of SERS substrates [37–39]. The interparticle distance of plasmonic nanoparticles on the beads' surface in their assembly create plasmonic hot spots, which leads to significant Raman enhancement [40]. Various methods have been proposed to immobilize a dense coverage of metal nanoparticles on the beads [26, 41–45]. Lee and coworkers reported a solvent controlled swelling and hetero coagulation method to synthesize highly light scattering metal nanoparticle-coated polystyrene (PS) beads for plasmonic and SERS applications [46, 47]. The immobilization of gold nanostars on PS beads to construct multifunctional SERS probes was also reported [48]. In addition, several other methods such as DNA mediated assembly, covalent coupling, and phase inversion precipitation methods have been explored for the fabrication of polymer-nanoparticle composite SERS substrates [26, 38, 41].

Most previous reports on core shell polymer nanoparticle composite systems focused on loading gold or silver nanospheres on PS beads [37, 41, 47]. In addition, while several of these methods were successful in increasing particle density on the beads' surface and creating plasmonic hot spots, beads remained isolated from one another, which limited the number of hot spots at the focal volume during SERS analysis. Here we report a DNA-based assembly of anisotropic gold nanoprisms and PS beads into a large ensemble of nanoprisms-coated PS beads for fabricating a large area of homogenous SERS substrate. Micron sized PS beads were first immobilized with a dense monolayer of nanoprisms to construct PS beads/nanoprisms conjugates through DNA hybridization. The initially formed PS beads/nanoprisms conjugates were subjected to heating below the melting transition point of the conjugates, followed by slow cooling, which induced the assembly of beads into larger PS beads/nanoprisms aggregates comprising 20–50 PS beads that are densely coated nanoprisms. The close packed arrangement of nanoprisms on PS beads' surface generated multiple hot spots in each bead. Additionally, assembling these nanoprisms loaded beads into a larger stack led to the formation a large areas of 3D SERS substrate with a larger number of plasmonic hot spots. SERS analysis of a probe molecule, methylene blue using 3D SERS substrate demonstrated an excellent EF (1.05×10^5) and detection limit of 10^{-10} M.

2. Result and discussion

Conjugation of nanoprisms to carboxylate-modified PS beads was carried out in two steps (scheme 1). In the first step, carboxylate-modified PS beads were conjugated with



Scheme 1. Schematic representation of DNA induced loading of gold nanoprisms onto PS beads.

an amine-modified thymine rich ss-DNA (DNA-A') via EDC/sulfo-NHS amide bond coupling chemistry.

Due to repulsive nature of negatively charged DNA linkers on the PS beads, DNA-A' functionalized PS beads were well dispersed in 0.01 M PBS, as shown by fluorescence microscopy image (figure S1 (available online at <https://stacks.iop.org/NANO/32/025506/mmedia>)) and as a single population distribution of PS beads in DLS size measurements, figure 1(a). In the second step, nanoprisms that are densely functionalized with adenine rich ss-DNA, DNA-A were coated on thymine rich DNA-A' functionalized PS beads using complementary DNA-DNA interaction between DNA-A and DNA-A'. The DNA-induced interaction between nanoprisms and PS beads resulted in the dense immobilization of nanoprisms on PS beads, leading to the formation of PS beads/nanoprisms conjugates, which were fully characterized by UV-Visible spectroscopy, dynamic light scattering (DLS) and SEM imaging. No PS beads/nanoprisms conjugation was observed when uncoated PS beads were mixed with uncoated nanoprisms under the same conditions, as shown by SEM imaging (Figure S2), indicating specific complementary DNA-DNA interaction between PS beads and nanoprisms in PS beads/nanoprisms conjugates.

To elucidate the effect of solution ionic strength on the DNA-mediated binding events between nanoprisms and PS beads, the conjugation of nanoprisms to PS beads was carried out at different salt concentrations, i.e. 0.1 M, 0.2 M and 0.3 M NaCl. Figure 1 shows the size distribution of PS beads/nanoprisms conjugates at different salt concentrations and representative SEM images showing the successful immobilization of nanoprisms onto PS beads. The first peak at around 100 nm in the DLS graph denotes the presence of unbound nanoprisms while the peak at around 1 μm hydrodynamic diameter represents PS beads/nanoprisms conjugates that consists of nanoprisms coated single bead or dimers of beads as shown in SEM images, Figures 1(b), (c) and S3, and the peak at around 5 μm hydrodynamic diameter denotes PS beads/nanoprisms conjugates, i.e. bead clusters, where 3–7 PS beads are bound together via the two major facets of nanoprisms, Figures 1(d) and S3.

The relatively larger DLS peak at around 100 nm hydrodynamic diameter for 0.1 M ionic strength compared to 0.2 M

and 0.3 M ionic strength indicates that there are more unbound nanoprisms for 0.1 M ionic strength and that the loading efficiency was indeed higher for 0.2 M and 0.3 M salt concentrations than 0.1 M salt concentration. However, the quantitative effect of solution ionic strength on the loading density of nanoprisms was apparently insignificant and there was no particular trend observed from SEM images. Previous studies on DNA-mediated loading of gold nanospheres on polymer beads demonstrated that the loading density of nanoparticles significantly increases with increasing salt concentration [41]. This difference in salt concentration dependence between the loading of anisotropic nanoprisms and nanosphere onto polymer beads could be attributed to the enhanced binding strength of nanoprisms, which is several million times higher than their nanosphere counterparts, stemming from the two major flat surfaces of prisms that can accommodate significantly more local DNA linker coating density than nanospheres [49].

However ionic strength did play a significant role in the growth of PS beads/nanoprisms clusters. As the salt concentration increased, the DLS peaks at larger diameters gradually increased, indicating the formation of larger number of bead clusters at higher salt concentration. This is because high solution ionic strength sufficiently screens the long-range electrostatic repulsion between beads and facilitated close contact between neighboring beads for short range hydrogen bonding between complementary DNA strands.

Figure 2 shows the UV-Vis absorption spectra of PS bead-/nanoprisms conjugates at different salt concentrations. The SPR absorbance of nanoprisms in the conjugates exhibits a significant red shift from the SPR absorbance of nanoprisms at 895 nm, Figure 2(a). The red shift in absorption band upon conjugation of nanoprisms to PS beads can be attributed to the interaction of nanoprisms with the PS beads as well as neighboring nanoprisms on PS beads surface. Absorption spectra also reveal the effect of ionic strength on the formation of PS beads/nanoprisms conjugates. For instance, the SPR band of nanoprisms were increasingly red shifted with increasing salt concentration from 0.1 M to 0.3 M, Figures 2(a) and S4 (UV-Vis spectra for loading smaller nanoprisms on PS beads at different salt concentrations), indicating that higher

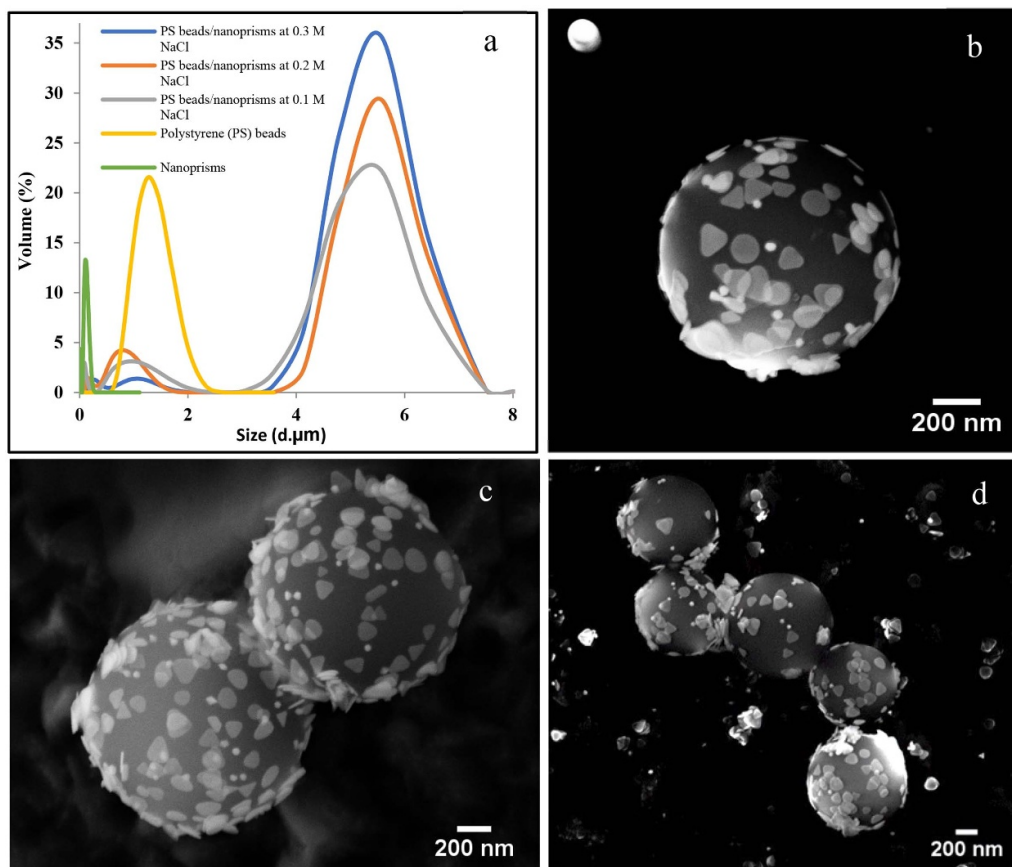


Figure 1. (a) DLS size characterization of salt effect in DNA induced binding between nanoprisms and PS microbeads, (b) and (c) representative SEM images of PS beads/nanoprisms conjugates, i.e. nanoprisms coated single or dimers of beads, and (d) representative SEM image of PS beads/nanoprisms conjugates, i.e. bead clusters.

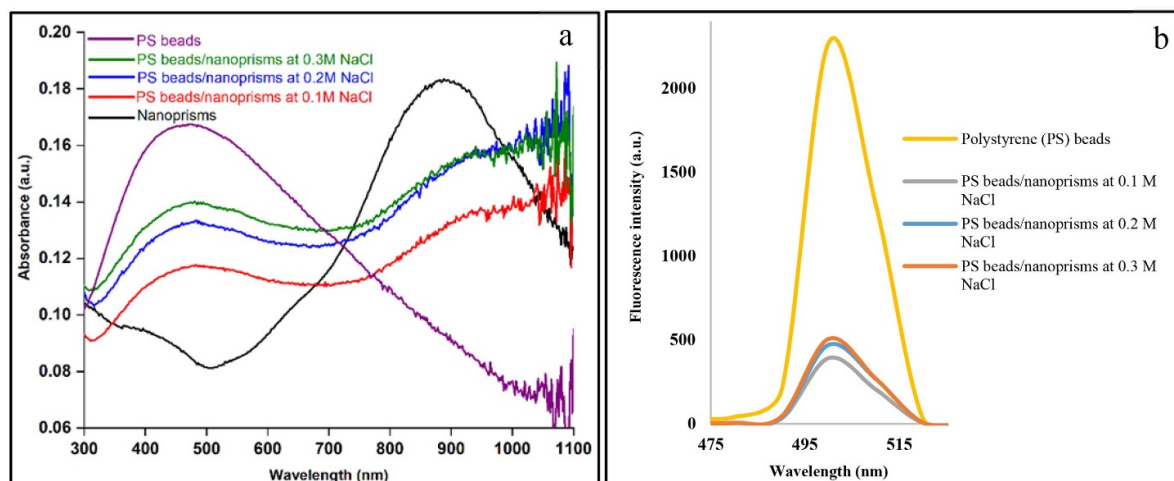


Figure 2. (a) UV-Vis characterization of salt effect in DNA induced binding between nanoprisms and PS beads, (b) fluorescence quenching of PS beads at different salt concentration.

ionic strength increases the formation of PS beads/nanoprisms cluster.

Gold nanoparticles can function as highly efficient fluorescence quencher, when the fluorophore is placed in proximity of nanoparticles [50–53]. This phenomenon of fluorescence quenching has been utilized for molecular sensing

applications [54] and energy transfer assays for the detection of biomolecules [55].

Moreover, conditional quenching or selective quenching of fluorescence can find applications in negative sensing [56]. The efficiency of fluorescence quenching by the nanoparticle is dependent on the distance between nanoparticle and

fluorescent object i.e. fluorophore and chromophore. Dulkeith *et al* investigated the mechanism of fluorescence quenching of cy5 for distances ranging from 2–16 nm between the nanoparticle and cy5 [57]. They showed that at all examined distances, the fluorescence intensity or efficiency of cy5 was reduced due to a reduced radiative decay rate of cy5. In this study, we used two 21-mer complementary ss-DNA strands, which are intertwined to form double helix in PS beads/nanoprisms conjugates. Therefore, the approximate distance between nanoprisms and PS beads would be around 7 nm, excluding salt-induced contraction of DNA. At all salt concentrations, the fluorescence intensity of the PS beads in PS beads/nanoprisms conjugates was significantly reduced compared to the intensity of uncoated PS beads of the same concentrations.

The emission spectra of fluorescent PS beads in PS beads/nanoprisms conjugates at various salt concentrations is shown in Figure 2(b). For all salt concentrations, the fluorescence of PS beads was almost quenched, and the intensity was reduced by almost 78% due to damping of PS beads' molecular dipole by the attached nanoprisms [58]. This could be due to phase induced suppression of radiative decay rate of the fluorescent PS beads, which are tangentially oriented to the nanoprisms surfaces [57, 59]. The effect of salt concentration on the fluorescence quenching was insignificant, which could be attributed to the lack of salt effect on the loading density of nanoprisms onto PS beads.

DNA-linked nanoparticle and microparticle aggregates exhibit cooperative melting behavior stemming from short range duplex to duplex interactions [60]. Upon heating above a characteristic temperature, which dissociates duplex DNA structures linking the particles into two complementary DNA strands, DNA-induced particle aggregates show a sharp melting transition, which is an indicative of dense functionalization of particles in DNA mediated particle assembly systems. In order to determine the characteristic melting temperature, PS beads/nanoprisms conjugates were heated from 45–90°C at a ramp rate of 0.25°C min⁻¹. During the heating process, the change in absorbance at surface plasmon resonance band (895 nm) of nanoprisms was monitored as a function of temperature. A control experiment was also carried out by similarly annealing a solution containing uncoated nanoprisms and uncoated PS beads. The sharp melting profile for the PS beads/nanoprisms conjugates (Figure 3(a)), as monitored via UV–vis spectroscopy, and the lack of such profile for the control experiment as shown in figure S5 confirmed the dense functionalization of DNA on nanoprisms and PS beads, and DNA-mediated interaction between PS beads and nanoprisms in PS beads/nanoprisms conjugates. Dehybridization of DNA linked PS beads/nanoprisms conjugates occurred over a narrow temperature range and the melting point was determined to be the inflection point at 78°C of the melting curve, approximately 37°C higher than T_m of the DNA linkers. This significant increase in T_m of PS beads/nanoprisms aggregates could be attributed to enhanced binding between nanoprisms and PS beads, and the formation of beads' cluster.

In order to create a large area of 3D homogenous SERS substrates, we adopted a DNA-induced nanoparticle/polymer

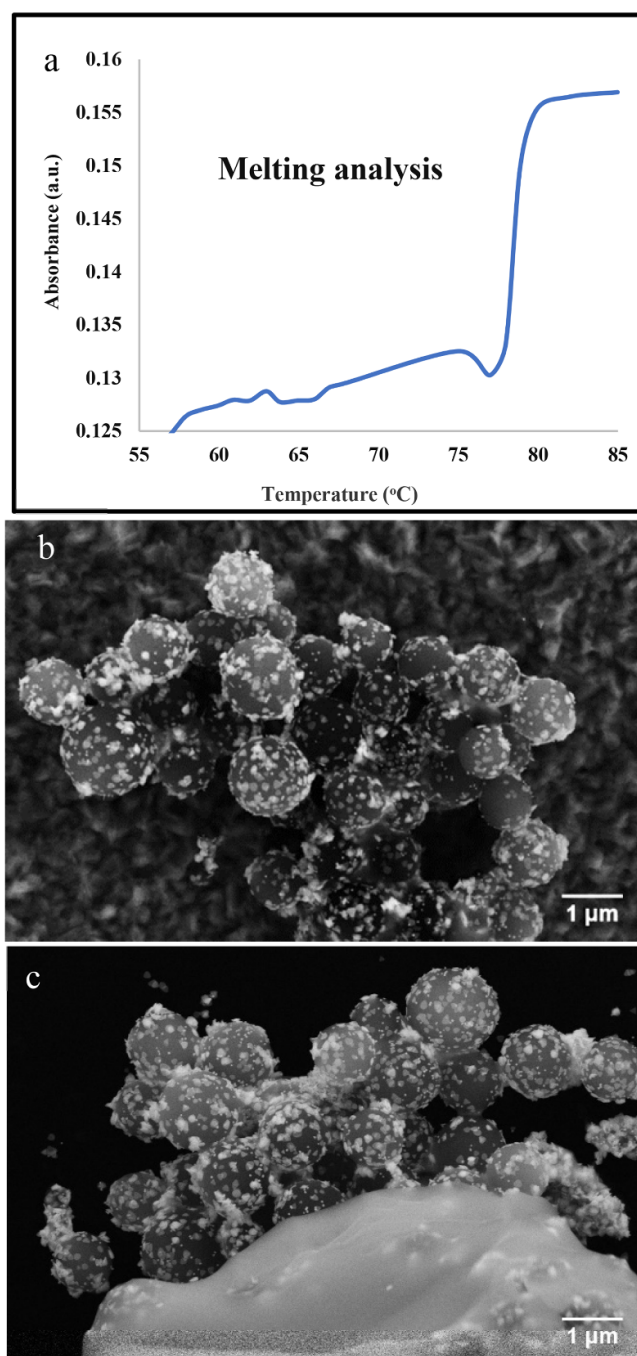


Figure 3. (a) Melting profile of PS beads/nanoprisms conjugates, monitored at 895 nm, SPR of nanoprisms, (b) and (c) representative SEM images of 3D PS beads/nanoprisms aggregates.

bead crystallization approach, i.e. thermal annealing followed by slow cooling. Initially formed PS beads/nanoprisms conjugates were heated to 65–70°C, which is below the melting point of the PS beads/nanoprisms conjugates, yet higher than the melting point of the DNA linkers. Thermal annealing below the melting point of the conjugates ensures the intactness of PS beads/nanoprisms conjugates, while slow cooling and heating above the T_m of the DNA strands allows the long range ordering of PS beads via DNA induced interaction between DNA-A coated nanoprisms and DNA-A'

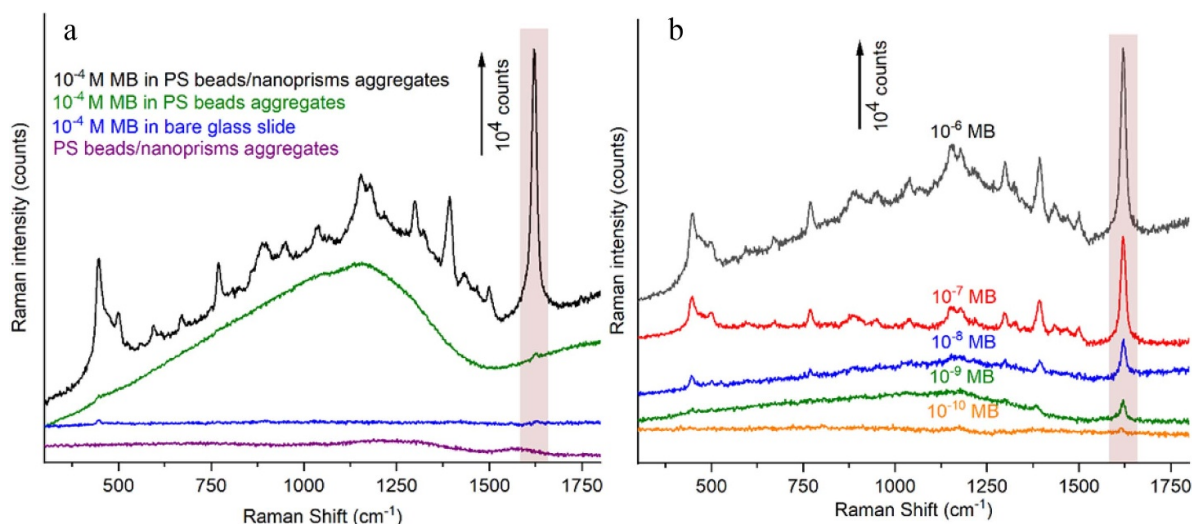


Figure 4. (a) Raman spectrum of PS beads/nanoprisms substrate (purple) and SERS spectra of MB adsorbed on glass substrate (blue), PS beads aggregates (green), & PS beads/nanoprisms aggregates (black), (b) SERS spectra of MB on 3D PS beads/nanoprisms aggregates at different concentrations.

coated PS beads, yielding a large ensemble/stack of PS beads (PS beads/nanoprisms aggregates). The resulting ensemble has a diameter ranging from 10–15 μm and consists of 20–50 PS beads that are bound through nanoprisms and DNA, Figures 3(b), (c) and S6. Each bead in the aggregates contains a number of closely spaced nanoprisms with various orientations such as tip-to-tip bowtie structures, tip-to-edge, edge-to-edge as well as interstitial orientations, with gap distances between prisms ranging from 1–20 nm. Depending on the gap and orientations, various arrangements of nanoprisms on the PS bead surfaces lead to varying degrees of plasmonic coupling and electromagnetic field enhancement in the vicinity of the nanoprisms' sharp edges and tips. Thus, the junctions of a large number of closely positioned nanoprisms in the 3D stacks of PS beads promotes the formation of high densities of plasmonic hot spots that could lead to strong SERS enhancement.

The performance of 3D PS beads/nanoprisms aggregates as a SERS substrate was evaluated using the common Raman reporter molecule methylene blue (MB). MB is chosen as the model compound for SERS analysis because of its well-known characteristic Raman bands. Figure 4(a) shows the Raman spectra of 3D PS beads/nanoprisms aggregates substrates without MB and 10^{-4} M aqueous solution of MB on three substrates: PS beads aggregates, glass substrate and 3D PS beads/nanoprisms aggregates. All the spectra were collected under the same conditions, using an excitation wavelength of 633 nm.

The Raman spectrum recorded for 10^{-4} M MB on the PS beads/nanoprisms aggregate substrate exhibit strongly enhanced Raman signals with good signal to noise ratio and characteristics peak positions for MB that are consistent with previous reports [61]. Some of the characteristic bands originating from MB are identified at 1621 cm^{-1} for (C–C) ring stretching, 1394 cm^{-1} for (C–N) symmetrical stretching, 1154 cm^{-1} for (C–H) in-plane bending, and

449 cm^{-1} for (C–N–C) skeletal deformation mode. These peaks were not observed for the Raman analysis of the SERS substrate without MB, indicating that they belong to MB. The significant enhancement of Raman intensity for the band at 1621 cm^{-1} indicates a perpendicular orientation and adsorption of probe molecules to the nanoprisms' surface, presumably through the fused phenyl and thiazine rings of the probe molecule [62].

While Raman analysis of 10^{-4} M MB on PS beads/nanoprisms aggregates substrate reveals a highly structured spectrum with well resolved characteristic peaks of MB, only two peaks with weak intensities were recorded for the same concentration of MB on PS bead aggregates and glass substrates, indicating that the 3D PS beads/nanoprisms aggregates is highly SERS active. The strong SERS enhancement for the 3D aggregates is attributed to the presence of plasmonic hot spots due to enhanced coupling and field enhancement from a close packed arrangement of nanoprisms. Notably, the Raman spectrum of MB on PS bead aggregates is masked by the auto-fluorescence of the PS beads, resulting in a larger fluorescence background and weaker Raman signal in the spectra. This is due to the fact that the laser excitation energy is close to the electronic transition energies of PS beads [21]. However, due to quenching of PS beads' fluorescence by the nanoprisms, the Raman spectra of MB on 3D PS beads/nanoprisms aggregates and 3D PS beads/nanoprisms aggregates themselves did not show a fluorescence background. As compared to SERS enhancement of PS beads/nanoprisms aggregates, the SERS intensity of 10^{-4} M MB, as shown in figure S7, obtained using randomly dispersed nanoprisms on glass substrate was substantially lower, which highlights the importance of densely packed arrangement of nanoprisms for high SERS efficiency.

To assess the reproducibility in SERS response of PS beads/nanoprisms aggregates, SERS intensity at 1621 cm^{-1} was measured for 10^{-7} M MB from 15 different PS beads/nanoprisms aggregates, Figure S8. The average signal intensity

at 1621 cm^{-1} for the PS beads/nanoprisms aggregates was 3580.4 counts with a coefficient of variation (CV) of only 18%, indicating that good reproducibility of the 3D nanoprisms superlattice as a SERS substrate. The molecular detection limit of 3D PS beads/nanoprisms aggregates was determined by recording SERS spectra of MB at different concentration varying from 10^{-6} to 10^{-10} M, Figure 4(b). The intensity of SERS peaks for MB expectedly decreased as the concentration of MB decreased. An obvious SERS peaks at 1621 cm^{-1} was still clearly visible at a very low MB concentration of 10^{-10} M, indicating high detection sensitivity of 3D PS beads/nanoprisms aggregates. And the SERS enhancement factor (EF) of 3D PS beads/nanoprisms aggregates was calculated from the SERS intensity of the prominent band at 1621 cm^{-1} (10^{-7} M MB) and Raman intensity of the corresponding band (10^{-4} M MB), considering bare glass substrate as the reference (see supporting info for details). The EF value is estimated to be 1.09×10^5 . The SERS performance of the 3D SERS substrate is comparable to or better than that of other nanoparticle-based plasmonic SERS substrates for the SERS analysis of MB [63–67].

3. Conclusion


In conclusion, we have demonstrated a DNA mediated self-assembly strategy for the fabrication of large area homogenous SERS substrates, i.e. PS beads/nanoprisms aggregates, from PS beads and gold nanoprisms. The conjugation of nanoprisms to PS beads was carried out using DNA–DNA hybridizations and the effect of solution ionic strength on the conjugation was investigated. No clear trend was observed for the effect of salt concentration on the loading density of nanoprisms on PS beads, but the size of nanoprisms loaded PS beads clusters increased with the increasing salt concentration as evidenced by the increasing red shift in the SPR of nanoprisms and DLS size distribution. The fluorescence intensity of fluorescent PS beads was reduced by 78% due to quenching effects of the nanoprisms conjugated to PS beads.

A SERS substrate was fabricated by assembling the initially formed PS bead/nanoprisms conjugates into a large 3D PS beads/nanoprisms aggregates via annealing the conjugates below the T_m (78°C), followed by slow cooling that facilitated the long-range interaction between PS beads and nanoprisms. The average size of PS beads/nanoprisms aggregates was found to be 10–15 μm in diameter and each aggregate consisted of 20–50 beads, where a large density of nanoprisms are arranged on the PS bead surfaces in various directions with varying interparticle distances, leading to the formation 3D plasmonic field with high density of plasmonic hot spots. The presence of such high-density hot spots led to homogeneous and high SERS enhancement. SERS measurements of methylene blue probe molecule on the 3D SERS substrates demonstrated excellent SERS enhancement ($<10^5$) with a limit of detection as low as 10^{-10} M concentration of MB. We believe that the conjugation and self-assembly approach we demonstrated here could be utilized for a number of applications including negative fluorescence-based detection and SERS based molecular sensing.

Notes

The authors declare no competing financial interests.

ORCID iDs

Mohammad Shahinur Rahaman  <https://orcid.org/0000-0003-0993-9367>

Noppadon Sathitsuksanoh  <https://orcid.org/0000-0003-1521-9155>

Martin G O'Toole  <https://orcid.org/0000-0001-9191-6601>

References

- [1] Giannini V, Fernández-Domínguez A I, Heck S C and Maier S A 2011 Plasmonic nanoantennas: fundamentals and their use in controlling the radiative properties of nanoemitters *Chem. Rev.* **111** 3888–912
- [2] Shegai T, Li Z, Dadosh T, Zhang Z, Xu H and Haran G 2008 Managing light polarization via plasmon-molecule interactions within an asymmetric metal nanoparticle trimer *Proc. Natl Acad. Sci. USA* **105** 16448–53
- [3] Mayer K M and Hafner J H 2011 Localized surface plasmon resonance sensors *Chem. Rev.* **111** 3828–57
- [4] Masson J F 2017 Surface plasmon resonance clinical biosensors for medical diagnostics *ACS Sens.* **2** 16–30
- [5] James K T, O'Toole M G, Patel D N, Zhang G, Gobin A M and Keynton R S 2015 A high yield, controllable process for producing tunable near infrared-absorbing gold nanoplates *RSC Adv.* **5** 12498–505
- [6] Sun M, Zhang Z, Zheng H and Xu H 2012 In-situ plasmon-driven chemical reactions revealed by high vacuum tip-enhanced Raman spectroscopy *Sci. Rep.* **2** 647
- [7] Morsin M, Mat Salleh M, Ali Umar A and Sahdan M Z 2017 Gold nanoplates for a localized surface plasmon resonance-based boric acid sensor *Sensors (Basel)* **17** 947
- [8] Gramotnev D K and Bozhevolnyi S I 2010 Plasmonics beyond the diffraction limit *Nat. Photon.* **4** 83–91
- [9] Xu H, Bjerneld E J, Käll M and Börjesson L 1999 Spectroscopy of single hemoglobin molecules by surface enhanced Raman scattering *Phys. Rev. Lett.* **83** 4357–60
- [10] Tian X, Tong L and Xu H 2013 New progress of plasmonics in complex metal nanostructures *Sci. China Phys. Mech. Astron.* **56** 2327–36
- [11] Reguera J, Langer J, de Aberasturi D J and Liz-Marzan L M 2017 Anisotropic metal nanoparticles for surface enhanced Raman scattering *Chem. Soc. Rev.* **46** 3866–85
- [12] Sajanlal P R, Sreeprasad T S, Samal A K and Pradeep T 2011 Anisotropic nanomaterials: structure, growth, assembly, and functions *Nano Rev.* **2** 5883
- [13] Nelayah J et al 2007 Mapping surface plasmons on a single metallic nanoparticle *Nat. Phys.* **3** 348–53
- [14] Brann T, Patel D, Chauhan R, James K T, Bates P J, Malik M T, Keynton R S and O'Toole M G 2016 Gold nanoplates as cancer-targeted photothermal actuators for drug delivery and triggered release *J. Nanomater.* **2016** 2036029
- [15] Patel D, James K T, O'Toole M, Zhang G, Keynton R S and Gobin A M 2015 A high yield, one-pot dialysis-based process for self-assembly of near infrared absorbing gold nanoparticles *J. Colloid Interface Sci.* **441** 10–16
- [16] Geng X, Leng W, Carter N A, Vikesland P J and Grove T Z 2016 Protein-aided formation of triangular silver nanoprisms with enhanced SERS performance *J. Mater. Chem. B* **4** 4182–90

- [17] Ou J, Tan H, Chen X and Chen Z 2018 DNA-assisted assembly of gold nanostructures and their induced optical properties *Nanomaterials*. **8** 994
- [18] Wei H and Xu H 2013 Hot spots in different metal nanostructures for plasmon-enhanced Raman spectroscopy *Nanoscale* **5** 10794–805
- [19] Michaels A M and Jiang B L 2000 Ag nanocrystal junctions as the site for surface-enhanced raman scattering of single rhodamine 6G molecules *J. Phys. Chem. B* **104** 11965–71
- [20] Hatab N A, Hsueh C-H, Gaddis A L, Retterer S T, Li J-H, Eres G, Zhang Z and Gu B 2010 Free-standing optical gold bowtie nanoantenna with variable gap size for enhanced raman spectroscopy *Nano Lett.* **10** 4952–5
- [21] Yang S, Li B, Slipchenko M N, Akkus A, Singer N G, Yeni Y N and Akkus O 2013 Laser wavelength dependence of background fluorescence in raman spectroscopic analysis of synovial fluid from symptomatic joints *J. Raman Spectrosc.: JRS* **44** 1089–95
- [22] Yilmaz M, Senlik E, Biskin E, Yavuz M S, Tamer U and Demirel G 2014 Combining 3-D plasmonic gold nanorod arrays with colloidal nanoparticles as a versatile concept for reliable, sensitive, and selective molecular detection by SERS *Phys. Chem. Chem. Phys.: PCCP* **16** 5563–70
- [23] Brolo A G, Arctander E, Gordon R, Leathem B and Kavanagh K L 2004 Nanohole-enhanced Raman scattering *Nano Lett.* **4** 2015–8
- [24] Gong J, Lipomi D J, Deng J, Nie Z, Chen X, Randall N X, Nair R and Whitesides G M 2010 Micro- and nanopatterning of inorganic and polymeric substrates by indentation lithography *Nano Lett.* **10** 2702–8
- [25] Chu Y, Wang D, Zhu W and Crozier K B 2011 Double resonance surface enhanced Raman scattering substrates: an intuitive coupled oscillator model *Opt. Express* **19** 14919–28
- [26] Belhout S A, Baptista F R, Devereux S J, Parker A W, Ward A D and Quinn S J 2019 Preparation of polymer gold nanoparticle composites with tunable plasmon coupling and their application as SERS substrates *Nanoscale* **11** 19884–94
- [27] Lim D-K, Jeon K-S, Kim H M, Nam J-M and Suh Y D 2010 Nanogap-engineerable Raman-active nanodumbbells for single-molecule detection *Nat. Mater.* **9** 60–67
- [28] Zhang Z, Zhang S and Lin M 2014 DNA-embedded Au–Ag core–shell nanoparticles assembled on silicon slides as a reliable SERS substrate *Analyst* **139** 2207–13
- [29] Kumar A, Hwang J-H, Kumar S and Nam J-M 2013 Tuning and assembling metal nanostructures with DNA *Chem. Commun.* **49** 2597–609
- [30] Tan S J, Campolongo M J, Luo D and Cheng W 2011 Building plasmonic nanostructures with DNA *Nat. Nanotechnol.* **6** 268–76
- [31] Chowdhury E, Grapperhaus C A and O'Toole M G 2020 Facet-selective asymmetric functionalization of anisotropic gold nanoprisms for Janus particle synthesis *J. Nanoparticle Res.* **22** 142
- [32] Thacker V V, Herrmann L O, Sigle D O, Zhang T, Liedl T, Baumberg J J and Keyser U F 2014 DNA origami based assembly of gold nanoparticle dimers for surface-enhanced Raman scattering *Nat. Commun.* **5** 3448
- [33] Pilo-Pais M, Watson A, Demers S, LaBean T H and Finkelstein G 2014 Surface-enhanced raman scattering plasmonic enhancement using DNA origami-based complex metallic nanostructures *Nano Lett.* **14** 2099–104
- [34] Zheng Y, Thai T, Reineck P, Qiu L, Guo Y and Bach U 2013 DNA-directed self-assembly of core-satellite plasmonic nanostructures: a highly sensitive and reproducible near-IR SERS sensor *Adv. Funct. Mater.* **23** 1519–26
- [35] Zhan P, Wen T, Wang Z-G, He Y, Shi J, Wang T, Liu X, Lu G and Ding B 2018 DNA origami directed assembly of gold bowtie nanoantennas for single-molecule surface-enhanced raman scattering *Angew. Chem. Int. Ed. Engl.* **57** 2846–50
- [36] Wei Q-H, Su K-H, Zhang X-X and Zhang X 2003 Engineering 'hot spots' for surface-enhanced Raman scattering *SPIE*
- [37] Zhang N C, Yu X, Hu J Q, Xue F and Ding E Y 2013 Synthesis of silver nanoparticle-coated poly(styrene-co-sulfonic acid) hybrid materials and their application in surface-enhanced Raman scattering (SERS) tags *RSC Adv.* **3** 13740–7
- [38] Trojanowska A, Pazos-Perez N, Panisello C, Gumi T, Guerrini L and Alvarez-Puebla R A 2015 Plasmonic-polymer hybrid hollow microbeads for surface-enhanced Raman scattering (SERS) ultradetection *J. Colloid Interface Sci.* **460** 128–34
- [39] Westcott S L, Oldenburg S J, Lee T R and Halas N J 1998 Formation and adsorption of clusters of gold nanoparticles onto functionalized silica nanoparticle surfaces *Langmuir* **14** 5396–401
- [40] Strozyk M S, de Aberasturi D J and Liz-Marzan L M 2018 Composite polymer colloids for SERS-based applications *Chem. Record (New York, NY)* **18** 807–18
- [41] Wu L-A, Li W-E, Lin D-Z and Chen Y-F 2017 Three-dimensional SERS substrates formed with plasmonic core-satellite nanostructures *Sci. Rep.* **7** 13066
- [42] Ishida T, Kuroda K, Kinoshita N, Minagawa W and Haruta M 2008 Direct deposition of gold nanoparticles onto polymer beads and glucose oxidation with H₂O₂ *J. Colloid Interface Sci.* **323** 105–11
- [43] Jeong C J, In I and Park S Y 2015 Facile preparation of metal nanoparticle-coated polystyrene beads by catechol conjugated polymer *Surface Interface Anal.* **47** 253–8
- [44] Belhout S A, Kim J Y, Hinds D T, Owen N J, Coulter J A and Quinn S J 2016 Multifunctional and robust composite materials comprising gold nanoparticles at a spherical polystyrene particle surface *Chem. Commun.* **52** 14388–91
- [45] Cassagneau T and Caruso F 2002 Contiguous silver nanoparticle coatings on dielectric spheres *Adv. Mater.* **14** 732–+
- [46] Lee J-H, Mahmoud M A, Sitterle V B, Sitterle J J and Meredith J C 2009 Highly scattering, surface-enhanced raman scattering-active, metal nanoparticle-coated polymers prepared via combined swelling–heteroaggregation *Chem. Mater.* **21** 5654–63
- [47] Lee J H, Mahmoud M A, Sitterle V, Sitterle J and Meredith J C 2009 Facile preparation of highly-scattering metal nanoparticle-coated polymer microbeads and their surface plasmon resonance *J. Am. Chem. Soc.* **131** 5048–9
- [48] Serrano-Montes A B et al 2016 Gold nanostar-coated polystyrene beads as multifunctional nanoprobes for SERS bioimaging *J. Phys. Chem. C* **120** 20860–8
- [49] Jones M R, Macfarlane R J, Prigodich A E, Patel P C and Mirkin C A 2011 Nanoparticle shape anisotropy dictates the collective behavior of surface-bound ligands *J. Am. Chem. Soc.* **133** 18865–9
- [50] Dulkeith E, Morteaux A C, Niedereichholz T, Klar T A, Feldmann J, Levi S A, van Veggel F C J M, Reinhoudt D N, Möller M and Gittins D I 2002 Fluorescence quenching of dye molecules near gold nanoparticles: radiative and nonradiative effects *Phys. Rev. Lett.* **89** 203002
- [51] Kang K A, Wang J, O'Toole M G, Nantz M, Moore J D, Laulhe S and Achifelu S et al 2012 Sensitivity enhancement of NIR fluorescence contrast agent utilizing gold nanoparticles *Oxygen Transport to Tissue Xxxiii. Advances in Experimental Medicine and Biology*, eds M Wolf, H U Bucher, M Rudin, S VanHuffel, U Wolf and D F Bruley et al (Berlin: Springer-Verlag Berlin) vol 737 pp 285–91
- [52] Dubertret B, Calame M and Libchaber A J 2001 Single-mismatch detection using gold-quenched fluorescent oligonucleotides *Nat. Biotechnol.* **19** 365–70

- [53] Wang J, O'Toole M, Massey A, Biswas S, Nantz M, Achifelu S and Kang K A *et al* 2011 Highly specific, NIR fluorescent contrast agent with emission controlled by gold nanoparticle *Oxygen Transport to Tissue Xxxii. Advances in Experimental Medicine and Biology*, eds J C LaManna, M A Puchowicz, K Xu, D K Harrison and D F Bruley (Boston, MA: Springer) **7012011** pp 149–54
- [54] Benincasa M, Pacor S, Gennaro R and Scocchi M 2009 Rapid and reliable detection of antimicrobial peptide penetration into gram-negative bacteria based on fluorescence quenching *Antimicrob. Agents Chemother.* **53** 3501–4
- [55] Maxwell D J, Taylor J R and Nie S 2002 Self-assembled nanoparticle probes for recognition and detection of biomolecules *J. Am. Chem. Soc.* **124** 9606–12
- [56] Hong B and Kang K A 2006 Biocompatible, nanogold-particle fluorescence enhancer for fluorophore mediated, optical immunosensor *Biosens. Bioelectron.* **21** 1333–8
- [57] Dulkeith E, Ringler M, Klar T A, Feldmann J, Muñoz Javier A and Parak W J 2005 Gold nanoparticles quench fluorescence by phase induced radiative rate suppression *Nano Lett.* **5** 585–9
- [58] Soller T, Ringler M, Wunderlich M, Klar T A, Feldmann J, Josel H P, Markert Y, Nichtl A and Kürzinger K 2007 Radiative and nonradiative rates of phosphors attached to gold nanoparticles *Nano Lett.* **7** 1941–6
- [59] Karthikeyan B 2010 Fluorescence quenching of rhodamine-6G in Au nanocomposite polymers *J. Phys. D: Appl. Phys.* **108** 084311
- [60] Jin R, Wu G, Li Z, Mirkin C A and Schatz G C 2003 What controls the melting properties of DNA-linked gold nanoparticle assemblies? *J. Am. Chem. Soc.* **125** 1643–54
- [61] Demirel G, Gieseck R L M, Ozdemir R, Kahmann S, Loi M A, Schatz G C, Facchetti A and Usta H 2019 Molecular engineering of organic semiconductors enables noble metal-comparable SERS enhancement and sensitivity *Nat. Commun.* **10** 5502
- [62] Roy S D, Ghosh M and Chowdhury J 2015 Adsorptive parameters and influence of hot geometries on the SER(R)S spectra of methylene blue molecules adsorbed on gold nanocolloidal particles *J. Raman Spectrosc.* **46** 451–61
- [63] Srichan C, Ekpanyapong M, Horprathum M, Eiamchai P, Nuntawong N, Phokharatkul D, Danvirutai P, Bohez E, Wisitsoraat A and Tuantranont A 2016 Highly-sensitive surface-enhanced raman spectroscopy (SERS)-based chemical sensor using 3D graphene foam decorated with silver nanoparticles as SERS substrate *Sci. Rep.* **6** 23733
- [64] Yilmaz M 2014 Combining 3-D plasmonic gold nanorod arrays with colloidal nanoparticles as a versatile concept for reliable, sensitive, and selective molecular detection by SERS *Phys. Chem. Chem. Phys.* **16** 5563–70
- [65] Xiao G-N and Man S-Q 2007 Surface-enhanced Raman scattering of methylene blue adsorbed on cap-shaped silver nanoparticles *Chem. Phys. Lett.* **447** 305–9
- [66] Xu T, Wang X, Huang Y, Lai K and Fan Y 2019 Rapid detection of trace methylene blue and malachite green in four fish tissues by ultra-sensitive surface-enhanced Raman spectroscopy coated with gold nanorods *Food Control.* **106** 106720
- [67] Li C, Huang Y, Lai K, Rasco B A and Fan Y 2016 Analysis of trace methylene blue in fish muscles using ultra-sensitive surface-enhanced Raman spectroscopy *Food Control.* **65** 99–105